The Astrophysical Journal, 865:159 (8pp), 2018 October 1 https://doi.org/10.3847/1538-4357/aadb87

Lorentz Invariance Violation Effects on Gamma–Gamma Absorption and Compton Scattering

Hassan Abdalla[1,2] and Markus Böttcher[1]
[1] Centre for Space Research, North-West University, Potchefstroom 2520, South Africa; hassanahh@gmail.com, Markus.Bottcher@nwu.ac.za
[2] Department of Astronomy and Meteorology, Omdurman Islamic University, Omdurman 382, Sudan
Received 2018 July 16; revised 2018 August 13; accepted 2018 August 16; published 2018 October 4

Abstract

In this paper, we consider the impact of the Lorentz invariance violation (LIV) on the $\gamma-\gamma$ opacity of the universe to very high energy (VHE) gamma-rays, compared to the effect of local underdensities (voids) of the extragalactic background light, and on the Compton scattering process. Both subluminal and superluminal modifications of the photon dispersion relation are considered. In the subluminal case, LIV effects may result in a significant reduction of the $\gamma-\gamma$ opacity for photons with energies $\gtrsim$10 TeV. However, the effect is not expected to be sufficient to explain the apparent spectral hardening of several observed VHE γ-ray sources in the energy range from 100 GeV to a few TeV, even when including effects of plausible inhomogeneities in the cosmic structure. Superluminal modifications of the photon dispersion relation lead to a further enhancement of the EBL $\gamma\gamma$ opacity. We consider, for the first time, the influence of LIV on the Compton scattering process. We find that this effect becomes relevant only for photons at ultra-high energies, $E \gtrsim 1$ PeV. In the case of a superluminal modification of the photon dispersion relation, both the kinematic recoil effect and the Klein–Nishina suppression of the cross section are reduced. However, we argue that the effect is unlikely to be of astrophysical significance.

Key words: astroparticle physics – cosmology: miscellaneous – galaxies: active – galaxies: jets – radiation mechanisms: non-thermal

1. Introduction

Recent astronomical observations and laboratory experiments appear to show hints that several phenomena in physics, astrophysics, and cosmology oppose a traditional view of standard-model physics (e.g., Riess et al. 1998; Furniss et al. 2013). This has motivated developments of modified or alternative theories of quantum physics and gravitation (e.g., Capozziello et al. 2013; Nashed & El Hanafy 2014; Wanas & Hassan 2014; Arbab 2015; Sami et al. 2018), generally termed *physics beyond the standard model* (e.g., Sushkov et al. 2011; Abdallah et al. 2013; El-Zant et al. 2015).

The special theory of relativity postulates that physical phenomena are identical in all inertial frames. Lorentz invariance is one of the pillars of modern physics and is considered to be a fundamental symmetry in Quantum Field Theory. However, several quantum-gravity theories postulate that familiar concepts such as Lorentz invariance may be broken at energies approaching the Planck energy scale, $E_P \sim 1.2 \times 10^{19}$ GeV (e.g., Amelino-Camelia et al. 1998; Jacob & Piran 2008; Liberati & Maccione 2009; Amelino-Camelia 2013; Tavecchio & Bonnoli 2016). Currently such extreme energies are unreachable by experiments on Earth, but for photons traveling over cosmological distances the accumulated deviations from Lorentz invariance may be measurable using Imaging Atmospheric Cherenkov Telescope facilities, in particular the future Cherenkov Telescope Array (CTA; e.g., Fairbairn et al. 2014; Lorentz & Brun 2017).

A deviation from Lorentz invariance can be described by a modification of the dispersion relation of photons and elementary particles such as electrons (e.g., Amelino-Camelia et al. 1998; Tavecchio & Bonnoli 2016). It is well known that the speed of light in a refractive medium depends on its wavelength, with shorter-wavelength (high-momentum) modes traveling more slowly than long-wavelength (low-momentum) photons. This effect is due to the sensitivity of light waves to the microscopic structure of the refractive medium. Similarly, in quantum-gravity theories, very high energy (VHE) photons could be sensitive to the microscopic structure of spacetime, leading to a violation of strict Lorentz symmetry. In that case, γ-rays with higher energy are expected to propagate more slowly than their lower-energy counterparts (e.g., Amelino-Camelia et al. 1998; Fairbairn et al. 2014; Tavecchio & Bonnoli 2016; Lorentz & Brun 2017). This would lead to an energy-dependent refractive index for light in vacuum. Therefore, the deviation from Lorentz symmetry can be measured by comparing the arrival time of photons at different energies originating from the same astrophysical source (e.g., Amelino-Camelia et al. 1998; Azzam et al. 2009; Tavecchio & Bonnoli 2016; Lorentz & Brun 2017; Wei et al. 2017).

Gamma-rays from objects located at a cosmological distance with energies greater than the threshold energy for electron–positron pair production can be annihilated due to $\gamma-\gamma$ absorption by low-energy extragalactic background photons (Nikishov 1962). The intergalactic $\gamma-\gamma$ absorption signatures have attracted great interest in astrophysics and cosmology due to their potential to indirectly measure the extragalactic background light (EBL) and thereby probe the cosmic star formation history (e.g., Biteau & Williams 2015). The predicted $\gamma-\gamma$ absorption imprints have been studied employing a variety of theoretical and empirical methods (e.g., Stecker 1969; Stecker et al. 1992; Hauser & Dwek 2001; Primack et al. 2005; Aharonian et al. 2006; Franceschini et al. 2008; Razzaque et al. 2009; Finke et al. 2010; Dominguez et al. 2011a; Gilmore et al. 2012).

Recent observations indicate that the VHE ($E > 100$ GeV) spectra of some distant ($z \gtrsim 0.5$) blazars, after correction for $\gamma-\gamma$ absorption by the EBL, appear harder than physically plausible (e.g., Furniss et al. 2013), although systematic studies of the residuals of spectral fits with standard EBL absorption on

large samples of VHE blazars (e.g., Biteau & Williams 2015; Mazin et al. 2017) reveal no significant, systematic anomalies on the entire samples. Nevertheless, the unexpected VHE γ-ray signatures seen in a few individual blazars are currently the subject of intensive research. Possible explanations of this spectral hardening include the hypothesis that the EBL density could be lower than expected from current EBL models (Furniss et al. 2013), an additional γ-ray emission component due to interactions along the line of sight of extragalactic ultra-high-energy cosmic rays (UHECRs) originating from the blazar (e.g., Essey & Kusenko 2010; Dzhatdoev 2015), the existence of exotic axion-like particles (ALPs) into which VHE γ-rays can oscillate in the presence of a magnetic field, thus enabling VHE photons to avoid $\gamma-\gamma$ absorption (e.g., Dominguez et al. 2011b; Dzhatdoev et al. 2017), EBL inhomogeneities (e.g., Furniss et al. 2015; Kudoda & Faltenbacher 2017; Abdalla & Böttcher 2017), and the impact of Lorentz invariance violation (LIV), which can lead to an increase of the $\gamma\gamma$ interaction threshold and thus to a reduction of cosmic opacity (especially at energies beyond $\sim$10 TeV), thus allowing high-energy photons to avoid $\gamma-\gamma$ absorption (e.g., Tavecchio & Bonnoli 2016).

In this paper, we discuss the reduction of the EBL $\gamma-\gamma$ opacity due to the existence of underdense regions along the line of sight to VHE gamma-ray sources (including contributions of both the direct starlight and reprocessed emission to the EBL) and compare the results with the LIV effect on cosmological photon propagation. We consider the LIV effect only for photons, but not for electrons, since the high-energy synchrotron spectrum of the Crab Nebula imposes a stringent constraint on any deviation of the electron dispersion relation from the Lorentz invariance (e.g., Jacobson et al. 2003).

LIV may also effect the process of Compton scattering, which is likely to be an important γ-ray production process in many astrophysical high-energy sources, such as accreting black hole binaries, pulsar wind nebulae, the jets from active galactic nuclei, and supernova remnants. In this paper, we discuss, to our knowledge for the first time, the impact of LIV on the Compton scattering process, both on energy–momentum conservation and on the Compton cross section.

In Section 2, we investigate the impact of the existence of cosmic voids along the line of sight to a distant VHE γ-ray source by using the EBL model developed by Finke et al. (2010). In Section 3, we review the impact of LIV on the EBL $\gamma\gamma$ opacity. In Section 4, we investigate LIV effects on the Compton scattering process, starting with basic conservation of energy and momentum, using the LIV-deformed dispersion relation for photons. The results are presented in Section 5, where we compare our results with predictions from standard quantum electrodynamics (QED). We summarize and discuss our results in Section 6. Throughout this paper, the following cosmological parameters are assumed: $H_0 = 70\,\mathrm{km\,s^{-1}\,Mpc^{-1}}$, $\Omega_m = 0.3$, $\Omega_\Lambda = 0.7$.

2. The Impact of a Cosmic Void on the EBL Energy Density Distribution

A generic study of the effects of cosmic voids along the line of sight to a distant astronomical object (e.g., blazar) on the EBL $\gamma-\gamma$ opacity has been done in Abdalla & Böttcher (2017). In that paper, the EBL was represented using the prescription of Razzaque et al. (2009), taking into account only the direct starlight contribution to the EBL. Assuming that a spherical cosmic void with radius R is located with its center at redshift z_v, between an observer and a VHE γ-ray source located at redshift z_s, the angle- and photon-energy-dependent EBL energy density at each point between the observer at redshift zero and the source was calculated. The cosmic void was represented by setting the star formation rate to 0 within the volume of the void. We found that the EBL deficit is proportional to the size of the void. Therefore, the effect of a number n of voids of radius R_1 is approximately the same as the effect of a large void with radius $R_n = nR_1$.

Since in the Razzaque et al. (2009) prescription only the direct starlight contribution to the EBL is considered, the work of Abdalla & Böttcher (2017) underpredicts the EBL $\gamma-\gamma$ opacity for VHE γ-rays with energies of $E \gtrsim 1$ TeV. Such VHE photons preferentially interact with longer-wavelength (IR–FIR) EBL photons, which are dominated by dust reprocessing of starlight, which is neglected in Razzaque et al. (2009). To study the impact of a cosmic void on the full EBL spectrum, from far-infrared through visible and extending into the ultraviolet, we used the EBL model of Finke et al. (2010), in which stars that evolved off the main sequence and re-emission of absorbed starlight by dust are considered. In all other aspects, we follow the formalism of Abdalla & Böttcher (2017).

One of the most complete public catalogs of cosmic voids (Sutter et al. 2012) is based on data from the Sloan Digital Sky Survey (SDSS), with effective radii of voids spanning the range 5–135h^{-1} Mpc. Also, there is evidence for a 300h^{-1} Mpc underdense region in the local galaxy distribution (e.g., Keenan et al. 2013). Recent measurements of optical and NIR anisotropies (e.g., Matsuura et al. 2017), at 1.1 and 1.6 μm, indicate that the resulting amplitude of relative EBL fluctuations is typically in the range of 10% to 30% (Zemcov et al. 2014).

The impact of an accumulation of cosmic voids amounting to a total size of radius $R = 1h^{-1}$ Gpc (where $h = H_0/(100\,\mathrm{km\,s^{-1}\,Mpc^{-1}})$) centered at redshift $z_v = 0.3$ is illustrated in Figure 1. The EBL energy density spectrum in the presence of voids (dashed lines) is compared to the homogeneous case (solid lines) at different points (redshifts, as indicated by the labels) along the line of sight in the left panel of Figure 1. The fractional difference between the homogeneous and the inhomogeneous case as a function of photon energy for various redshifts along the line of sight is presented in the right panel of Figure 1. We notice that the EBL deficit is smaller for low-energy (IR) photons than for optical—ultraviolet photons. This is because the UV EBL is dominated by hot, young stars, thus more strongly reflecting the local effect of the void. Since in this work we set only the star formation rate inside the void equal to zero, dust reprocessing of starlight produced outside the void still takes place inside the void. As can be seen from Figure 1, with our choice of a void configuration, the impact of underdense regions is comparable to the measured optical and NIR anisotropy (Zemcov et al. 2014). The impact of the EBL deficit due to the cosmic voids on the EBL $\gamma-\gamma$ opacity will be presented in Section 5.1.

3. Lorentz Invariance Violation: Cosmic Opacity

In this section, we review the imprints of LIV on the cosmic $\gamma-\gamma$ opacity, primarily based on the work by Tavecchio & Bonnoli (2016). The results will be compared to the imprints of EBL inhomogeneities discussed in the previous section. The

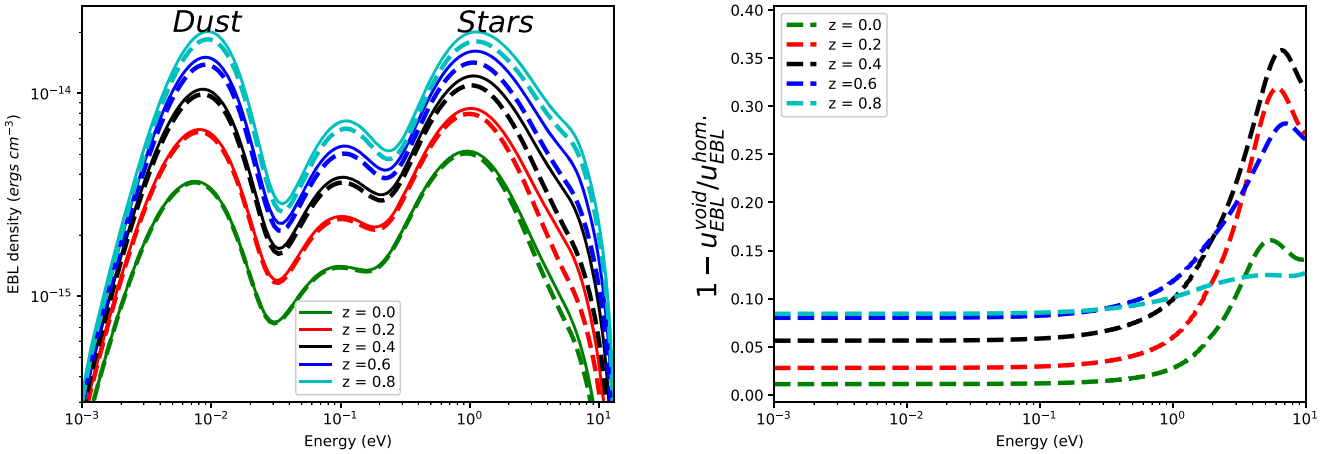

Figure 1. Left panel: differential EBL photon energy density as a function of distance (redshift) along the line of sight. The solid lines represent the homogeneous case ($R = 0$), and the dashed lines represent the EBL energy density considering an accumulation of about 10 voids of typical sizes with radius $R = 100h^{-1}$ Mpc centered at redshift $z_v = 0.3$. The EBL energy density increases with redshift because of the star formation rate increasing with redshift at low redshifts (e.g., Cole et al. 2001). Right panel: relative EBL energy density deficit due to the presence of a void for the same cases as represented in the left panel. $U_{\rm EBL}^{\rm void}$ and $U_{\rm EBL}^{\rm hom}$ are the EBL energy densities considering the cosmic void case and the homogeneous case, respectively. As expected, the maximum EBL energy density deficit occurs around the center of the voids ($z = 0.3$), and the EBL energy density deficit beyond the center of the cosmic voids is greater than the deficit in front of it, comparing points at the same distance from the voids center, due to the star formation rate increasing with redshift.

deviation from Lorentz symmetry can be described by a modification of the dispersion relation of photons and electrons (e.g., Amelino-Camelia et al. 1998; Tavecchio & Bonnoli 2016):

$$E^2 = p^2c^2 + m^2c^4 + S\,E^2\left(\frac{E}{E_{\rm LIV}}\right)^n, \qquad (1)$$

where c is the conventional speed of light in vacuum, "$S = -1$" represents a subluminal scenario (decreasing photon speed with increasing energy), and "$S = +1$" represents the superluminal case (increasing photon speed with increasing energy). The characteristic energy $E_{\rm LIV}$ is parameterized as a fraction of the Planck energy, $E_{\rm LIV} = E_P/\xi_n$, where the dimensionless parameter ξ_n and the order of the leading correction n depend on particle type and theoretical framework (e.g., Amelino-Camelia et al. 1998; Tavecchio & Bonnoli 2016). A value of $E_{\rm LIV} \sim E_P$ (i.e., $\xi_1 = 1$) has been considered to be the physically best motivated choice (e.g., Liberati & Maccione 2009; Fairbairn et al. 2014; Tavecchio & Bonnoli 2016). This is consistent with the results of Biteau & Williams (2015), which constrained $E_{\rm LIV} > 0.65\,E_P$. Some authors (e.g., Schaefer 1998; Biller et al. 1999) argue that the best constraint from the current data is $\xi_1 \leqslant O(1000)$.

In the literature (e.g., Tavecchio & Bonnoli 2016), usually only the subluminal case is considered for the LIV effect on $\gamma\gamma$ absorption, as this is the case that could lead to an increase of the $\gamma\gamma$ interaction threshold and, consequently, a decrease of the opacity. In this work, for completeness, we consider both the subluminal and superluminal cases.

Based on the revised dispersion relation (1) with $n = 1$, the modified pair-production threshold energy $\epsilon_{\rm min}$ can be written as (e.g., Tavecchio & Bonnoli 2016)

$$\epsilon_{\rm min} = \frac{m^2c^4}{E_\gamma} - S\,\frac{E_\gamma^2}{4E_{\rm LIV}}. \qquad (2)$$

Using Equation (2), the target photon energy threshold for pair production as a function of the γ-ray photon energy for the subluminal and the superluminal cases is illustrated in Figure 2.

Also from Equation (1), an effective mass term for photons can be defined as (e.g., Liberati & Maccione 2009; Tavecchio & Bonnoli 2016)

$$(m_\gamma\,c^2)^2 \equiv S\,\frac{E^3(1+z)^3}{E_{\rm LIV}}. \qquad (3)$$

Following Fairbairn et al. (2014) and Tavecchio & Bonnoli (2016), we assume that the functional form of the $\gamma - \gamma$ cross section (as a function of the center-of-momentum energy squared s) remains unchanged by the LIV effect, and only the expression for s is modified. The optical depth at the energy E_γ and for γ-ray photons from a source at redshift z_s can thus be evaluated as (Fairbairn et al. 2014; Tavecchio & Bonnoli 2016)

$$\tau_{\gamma\gamma}(E_\gamma, z_s) = \frac{c}{8E_\gamma^2}\int_0^{z_s}\frac{dz}{H(z)(1+z)^3}\int_{\epsilon_{\rm min}}^{\infty}\frac{n(\epsilon, z)}{\epsilon^2}\int_{s_{\rm min}}^{s(z)_{\rm max}} \times [s - (m_\gamma\,c^2)^2]\sigma_{\gamma\gamma}(s)ds, \qquad (4)$$

where $H(z) = H_0\sqrt{[\Omega_m(1+z)^3 + \Omega_\Lambda]}$, $s_{\rm min} = 4\,(m_e\,c^2)^2$, and $s(z)_{\rm max} = 4\epsilon E_\gamma\ (1+z)+(m_\gamma\,c^2)^2$. $n(\epsilon,z)$ is the EBL photon energy density as a function of redshift z and energy ϵ, and $\sigma_{\gamma\gamma}(s)$ is the total pair-production cross section as a function of the modified square of the center-of-mass energy $s = (m_\gamma\,c^2)^2 + 2\epsilon E_\gamma(1 - \cos(\theta))$, where θ is the angle between the soft EBL photon of energy ϵ and the VHE γ-ray photon. Obviously, when $E_{\rm LIV} \longrightarrow \infty$, the standard relations are recovered.

By using Equation (4) with the EBL model by Finke et al. (2010), we calculate the optical depth for VHE γ-ray photons from a source at redshift 0.6. The comparison with the standard case (homogeneous EBL, no LIV) and with the effect of EBL inhomogeneities (as discussed in Section 2) is presented in Section 5.1.

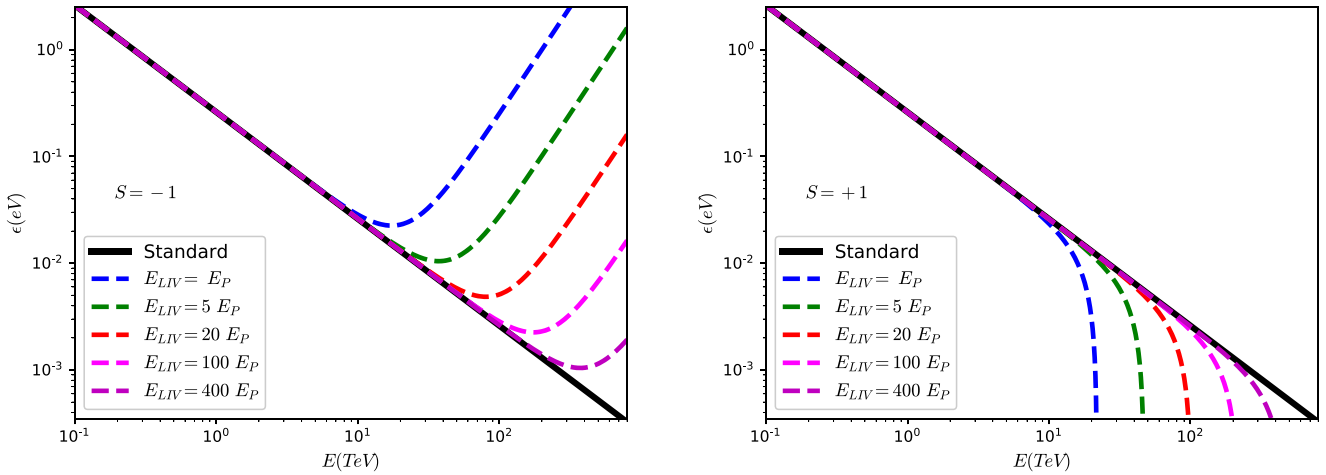

Figure 2. Left panel: photon target energy at threshold for pair production as a function of γ-ray photon energy, for the subluminal case. The black solid line represents the case of standard QED, and the dashed lines show the LIV-modified threshold for different values of $E_{\rm LIV}$. Right panel: same as the left panel, but for the superluminal case.

4. Lorentz Invariance Violation: Compton Scattering

One of the most important fundamental high-energy radiation mechanisms is Compton scattering, the process by which photons gain or lose energy from collisions with electrons. In the Compton scattering processes, the energy of a scattered photon $E_{\gamma f}$ follows from momentum and energy conservation:

$$(E_{\gamma i}/c, \vec{P_{\gamma i}}) + (E_{ei}/c, \vec{P_{ei}}) = (E_{\gamma f}/c, \vec{P_{\gamma f}}) + (E_{ef}/c, \vec{P_{ef}}), \quad (5)$$

which is assumed to still hold even in a Lorentz invariance violating framework. In Equation (5), $E_{\gamma i}$, $E_{\gamma f}$ and E_{ei}, E_{ef} are initial and final energies for the photon and electron, respectively, and $\vec{P_{\gamma i}}$, $\vec{P_{\gamma f}}$ and $\vec{P_{ei}}$, $\vec{P_{ef}}$ are initial and final momenta for the photon and electron, respectively. To consider the LIV effect, we consider the first-order correction $n = 1$ in the modified dispersion relation (1):

$$E_\gamma^2 = p_\gamma^2 c^2 + S\,\frac{E_\gamma^3}{E_{\rm LIV}}. \quad (6)$$

As motivated in the Introduction, and consistent with our treatment of LIV on the EBL opacity in Section 3, we consider LIV only for photons, not for electrons. Substituting for E_{ef} using the standard electron dispersion relation and momentum conservation (considering that in the electron rest frame, $p_{e,i} = 0$), the energy conservation part of Equation (5) can be written as

$$E_{\gamma f} = E_{\gamma i} + E_{ei} - \sqrt{c^2(p_{\gamma i} - p_{\gamma f})^2 + (m_e c^2)^2}\,. \quad (7)$$

Squaring and rearranging Equation (7), expressing all photon momenta in terms of energies using the dispersion relation (6) yields

$$2E_{\gamma i}E_{\gamma f} + 2(E_{\gamma f} - E_{\gamma i})m_e c^2 = S\left(\frac{E_{\gamma i}^3}{E_{\rm LIV}} + \frac{E_{\gamma f}^3}{E_{\rm LIV}}\right) + 2\,\mu\,\sqrt{E_{\gamma i}^2 - S\,\frac{E_{\gamma i}^3}{E_{\rm LIV}}}\sqrt{E_{\gamma f}^2 - S\,\frac{E_{\gamma f}^3}{E_{\rm LIV}}}, \quad (8)$$

where $\mu = \cos\theta$ is the cosine of the scattering angle in the electron rest frame. In the limit $E_{\rm LIV} \gg E_\gamma$, the square-root expressions in Equation (8) can be simplified to

$$\sqrt{E_\gamma^2 - S\,\frac{E_\gamma^3}{E_{\rm LIV}}} \approx E_\gamma\left(1 - S\,\frac{E_\gamma}{2E_{\rm LIV}}\right). \quad (9)$$

Thus, to lowest order in $\boldsymbol{E}_\gamma/\,\boldsymbol{E}_{\rm LIV}$, Equation (8) can be written as

$$2E_{\gamma i}E_{\gamma f} + 2(E_{\gamma f} - E_{\gamma i})m_e c^2 = S\left(\frac{E_{\gamma i}^3}{E_{\rm LIV}} + \frac{E_{\gamma f}^3}{E_{\rm LIV}}\right) + 2\mu E_{\gamma i}E_{\gamma f}\left(1 - S\,\frac{E_{\gamma i}}{2E_{\rm LIV}} - S\,\frac{E_{\gamma f}}{2E_{\rm LIV}}\right). \quad (10)$$

Equation (10) is solved numerically to find the scattered photon energy $E_{\gamma f}$ as a function of initial photon energy $E_{\gamma i}$ and scattering angle $\theta = \cos^{-1}\mu$. Results are presented in Section 5.2.

From QED, the Klein–Nishina cross section $\sigma_{\rm KN}$ can be written as

$$\sigma_{\rm KN} = \int \frac{d\sigma_{\rm KN}}{d\Omega} d\Omega = \int \frac{r_e^2}{2}\left(\frac{E_{\gamma f}}{E_{\gamma i}}\right)^2\left(\frac{E_{\gamma i}}{E_{\gamma f}} + \frac{E_{\gamma f}}{E_{\gamma i}} - \sin^2\theta\right)d\Omega, \quad (11)$$

where $\frac{d\sigma_{\rm KN}}{d\Omega}$ is the differential Klein–Nishina cross section, $d\Omega$ is the solid angle, and r_e is the classical electron radius.

As for our considerations of the LIV effect on the $\gamma-\gamma$ opacity, we assume that the functional dependence of the Klein–Nishina cross section on the incoming and scattered photon energies remains unaffected. Thus, in order to modify the Klein–Nishina cross section considering the LIV effect, we use the scattered photon $E_{\gamma f}$ from the solution of Equation (10) in the Klein–Nishina formula (11) and integrate numerically. The results of this integration compared with the standard QED case are presented in Section 5.2.

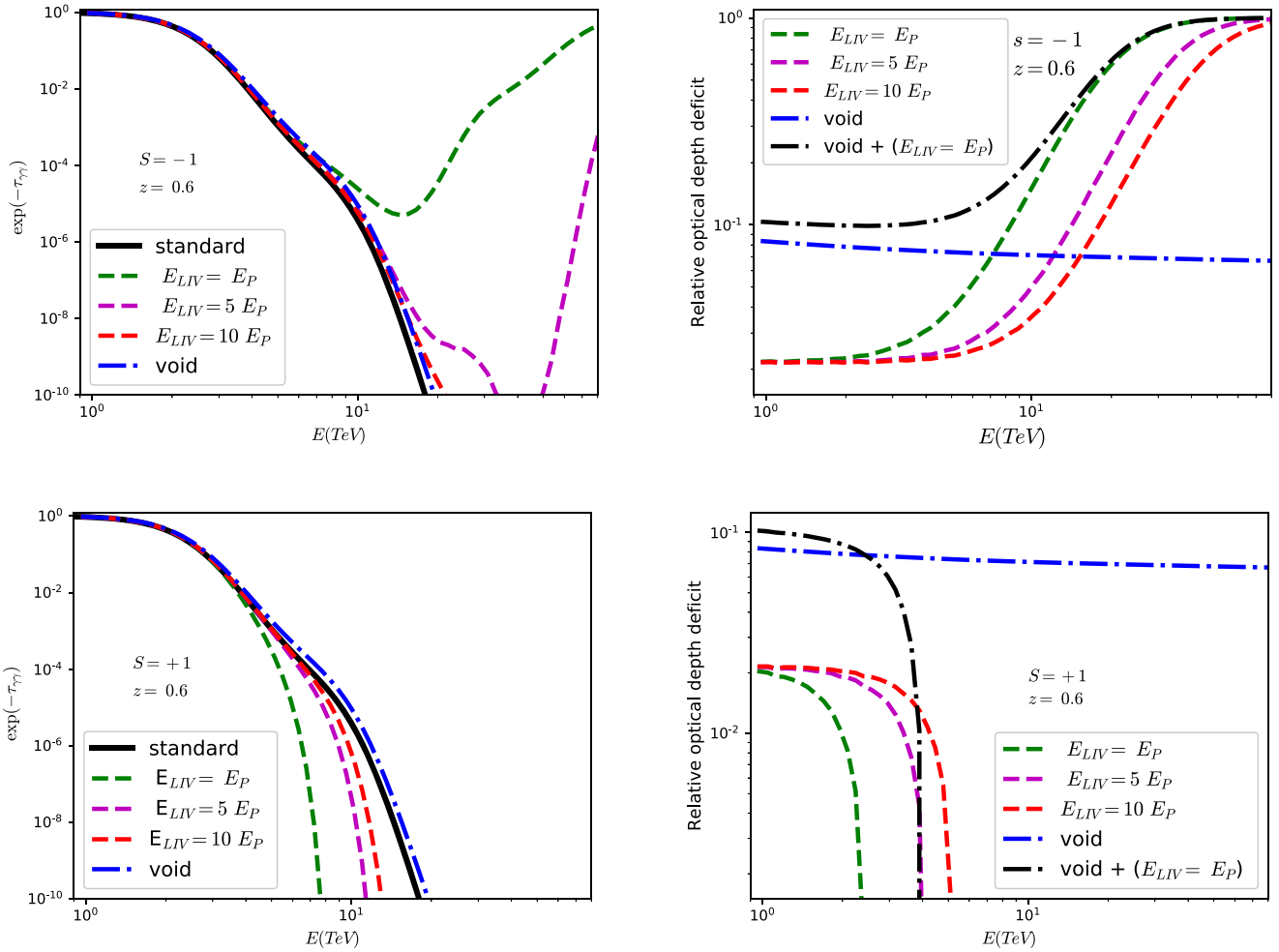

Figure 3. Left panels: absorption coefficient $\exp(-\tau_{\gamma\gamma})$ as a function of energy for VHE γ-rays from a source at redshift $z_s = 0.6$, using the EBL model of Finke et al. (2010). The black solid line represents the case of standard QED; the dashed lines show the LIV-modified coefficient for different values of $E_{\rm LIV}$, for the subluminal case (top panel) and the superluminal case (bottom panel). The blue dotted–dashed line represents the case of standard QED and EBL energy density calculated by considering an accumulation of 10 voids of typical sizes with radius $R = 100\ h^{-1}$ Mpc along the line of sight, centered at redshift $z_v = 0.3$. Right panels: relative optical depth deficit as a function of energy for VHE γ-rays for the same cases as in the left panel. The relative optical depth deficit is defined as $(1 - \tau_{\gamma\gamma}^{\rm DFS}/\tau_{\gamma\gamma}^{\rm Stand.})$, where $\tau_{\gamma\gamma}^{\rm Stand.}$ represents the optical depth calculated in standard QED and using the homogeneous EBL energy density distribution, and $\tau_{\gamma\gamma}^{\rm DFS}$ represents the optical depth calculated including the effects of cosmic voids (blue dashed–dotted line) or of LIV (dashed lines). The black dotted–dashed line represents the relative optical depth deficit due to the combined effect of LIV and EBL inhomogeneities.

5. Results and Discussion

In this section, we present the results for representative test cases for the LIV effect on the cosmic $\gamma - \gamma$ opacity, compared to the standard Lorentz invariance case and the suppression of the opacity due to EBL inhomogeneities, and on the Compton scattering process, compared to the standard-model case.

5.1. EBL Absorption

To study the opacity or transparency of the universe to VHE γ-ray photons from distant sources (e.g., blazars) due to their interaction with intergalactic EBL photons, we compare the effects of the EBL inhomogeneities due to the presence of cosmic voids to those of the LIV effect. Figure 3 shows the absorption coefficient $\exp(-\tau_{\gamma\gamma})$ as a function of energy for VHE gamma-rays from a source at redshift $z_s = 0.6$. The standard-model QED case is represented by the black solid line. The impact of an EBL underdensity (for parameters as used in Figure 1) is illustrated by dotted–dashed lines, and the LIV effect is represented by dashed lines for different values of the characteristic LIV energy scale $E_{\rm LIV} = E_P/\xi_1$. Note that the standard case without LIV is recovered for $E_{\rm LIV} \longmapsto \infty$. The reduction of the EBL $\gamma - \gamma$ opacity due to plausible EBL inhomogeneities is only of the order of $\lesssim$10% and decreases with energy. The LIV effect is negligibly small for energies below about 5 TeV, but the cosmic opacity for VHE γ-rays with energies $\gtrsim$10 TeV can be strongly reduced for the subluminal case and increased for the superluminal case. Therefore, if LIV is described by the subluminal dispersion relation ($S = -1$), one may expect VHE γ-ray photons beyond 10 TeV to be observable even from distant astrophysical sources.

However, the spectral hardening of several observed VHE gamma-ray sources with energy from 100 GeV up to a few TeV (e.g., PKS 1424+240) still remains puzzling. Compared to the Finke et al. (2010) EBL absorption model for an object at a redshift of $z_s \sim 0.6$, the opacity would have to be reduced by $\gtrsim$60% in order to explain the spectral hardening of the VHE

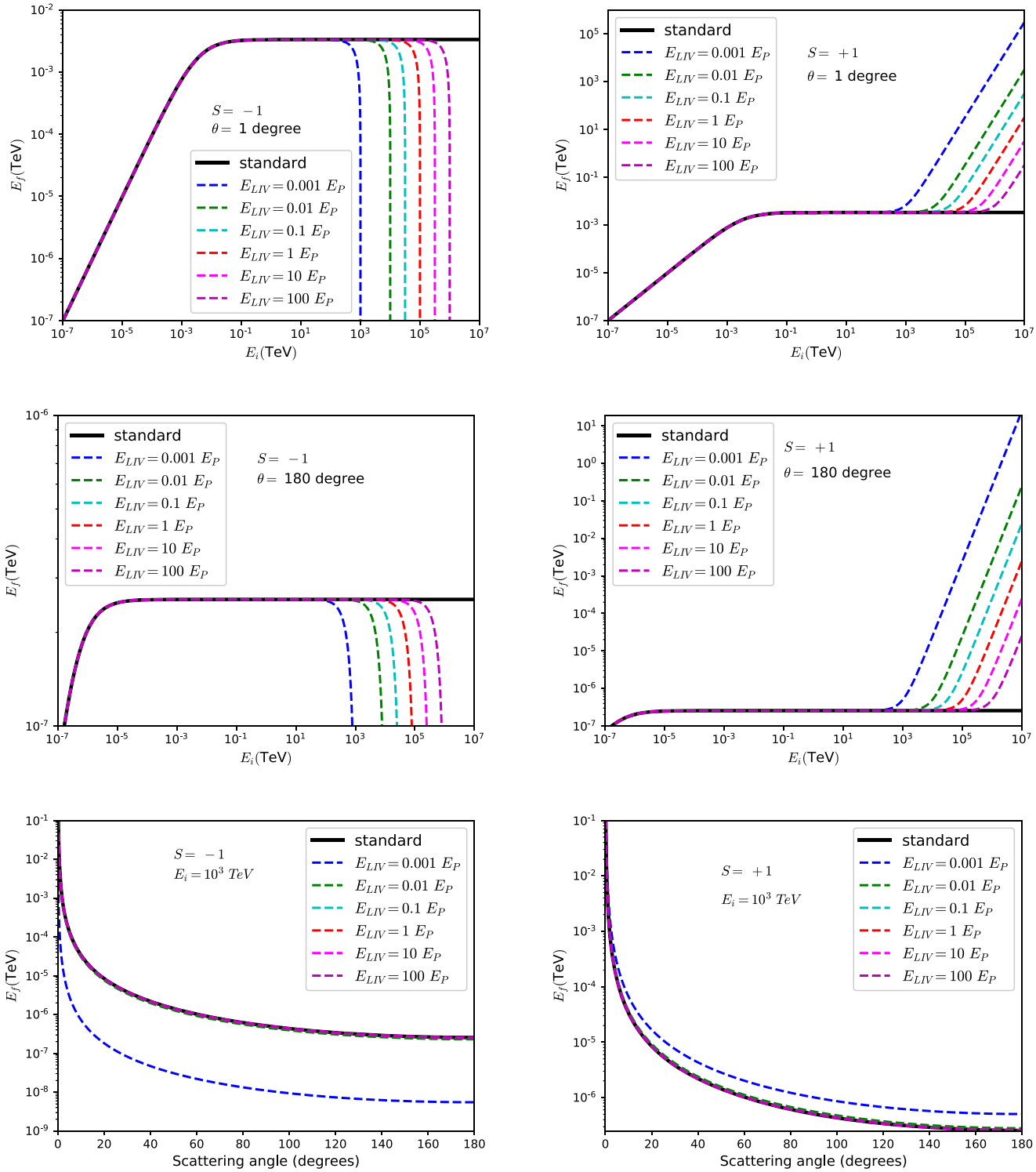

Figure 4. Top and middle panels: scattered photon energies $E_{\gamma,f}$ as a function of incoming photon energy $E_{\gamma,i}$, for scattering angles of 1° and 180°, respectively. The black solid line represents the case of standard QED; the dashed lines show the LIV effect for different values of $E_{\rm LIV}$, for a subluminal case (left) and superluminal case (right). Bottom panels: scattered photons energies E_f vs. scattering angle, for an incoming photon energy of $E_i = 1$ PeV in the subluminal case (left) and superluminal case (right). The black solid line represents the case QED; the dashed lines illustrate the LIV effect for different values of $E_{\rm LIV}$.

spectrum of PKS 1424+240 with standard emission mechanisms. Even if we consider the combined effects of EBL underdensities and LIV, as represented by the solid line in the right panel of Figure 3, the relative optical depth $\tau\gamma\gamma$ deficit is only around 10% in the energy range from hundreds of GeV to a few TeV.

5.2. Compton Scattering

The LIV effect on the Compton scattering process has been evaluated as described in Section 4. To assess the importance of LIV signatures, we have evaluated this effect for a large range of values of $E_{\rm LIV}$. All calculations are done in the electron rest frame.

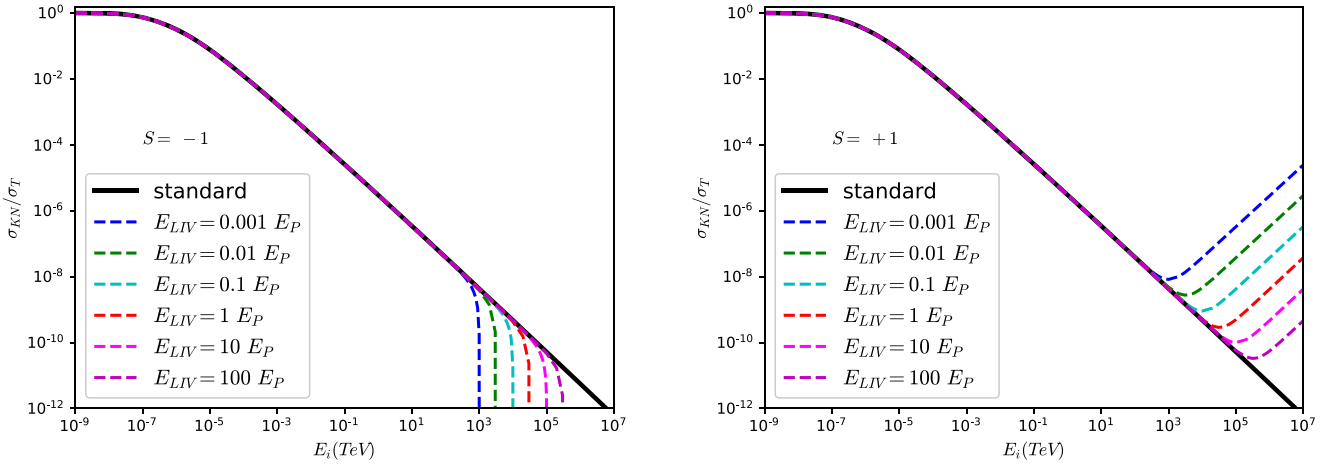

Figure 5. Total Klein–Nishina cross section $\sigma_{\rm KN}$ (in the units of σ_T) as a function of the incoming photon energy $E_{\gamma,i}$. The black solid line represents the case of QED; the dashed lines show the LIV-modified Klein–Nishina cross section for different values of $E_{\rm LIV}$, for the subluminal (left panel) and superluminal (right panel) cases.

Figure 4 illustrates the effect of LIV on the scattered photon energies as a function of the incoming photon energies E_i for two representative scattering angles (1° and 180°—top and middle panels) for different values of $E_{\rm LIV}$, as well as the scattered photon energies as a function of the scattering angle θ for one representative incoming photon energy (10^3 TeV—bottom panels). The subluminal cases are illustrated in the left panels, the superluminal cases in the right panels. In the standard QED case (black solid curves), the kinematic constraints (recoil) lead to the well-known leveling off of the scattered photon energies at a value of $E_{\gamma,f} \sim m_e c^2/(1-\cos\theta)$.

In Figure 5, we illustrate the LIV effect on the total Klein–Nishina cross section $\sigma_{\rm KN}$ (in units of σ_T), plotted as a function of the incoming photon energy $E_{\gamma,i}$. The black solid line represents the case of standard QED and the dashed lines show the modified Klein–Nishina cross section for different values of $E_{\rm LIV}$, calculated as described in Section 4. Again, the subluminal and superluminal cases are illustrated in the left and right panels, respectively.

From Figures 4 and 5 we see that LIV signatures in the Compton scattering processes are expected to be important only for very large incoming photon energies, $E_{\gamma,i} \gtrsim 1$ PeV. In the superluminal case, the scattered photon energies are larger than expected in the standard case, while in the subluminal case, the scattered photon energies are further reduced. Although the impact of this effect on the scattered photon energy is large for photons with energy $E_{\gamma,i} > 10$ PeV, even in the superluminal case the scattered photon energy $E_{\gamma f}$ is still much smaller than the incoming photon energy $E_{\gamma,i}$. This indicates that the electron recoil effect is still substantial, as expected, but strongly reduced/increased compared to standard-model kinematics, in the superluminal/subluminal case, respectively. Equally, at energies $E_{\gamma,i} \gtrsim 1$ PeV the Klein–Nishina cross section gradually recovers from the standard-model Klein–Nishina suppression (which sets in at $E_{\gamma,i} \sim m_e c^2$) in the superluminal case, but is expected to remain suppressed to $\sigma_{\rm KN} \lesssim 10^{-6}\,\sigma_T$ for photon energies below ∼1 EeV (in the electron rest frame) for any plausible choice of $E_{\rm LIV}$. In the subluminal case, Compton scattering of photons at energies $E_{\gamma,i} \gtrsim 1$ PeV is expected to be strongly suppressed, far beyond the standard QED Klein–Nishina suppression.

6. Summary and Conclusions

We have presented calculations of the modification of the EBL $\gamma-\gamma$ opacity for VHE γ-ray photons from sources at cosmological distances by considering two effects: the impact of underdensities (voids) along the line of sight to the source and the LIV effect. For the LIV effect, we considered both a subluminal and a superluminal modification of the dispersion relation for photons. We found that the reduction of the optical depth due to the existence of cosmic voids is insignificant for realistic parameters of the void and is thus insufficient to explain the unexpected spectral hardening of the VHE spectra of several blazars. The effect of LIV becomes important only at γ-ray energies above ∼10 TeV, where the $\gamma\gamma$ interaction threshold is increased and, consequently, the EBL opacity is reduced in the subluminal case. The opposite effect (reduced pair-production threshold and increased EBL opacity) results in the superluminal case. The effect is negligible for VHE spectra in the range ∼100 GeV—a few TeV. However, these results suggest that, if LIV is manifested by a subluminal modification by the photon dispersion relation, VHE γ-ray sources may be detectable at cosmological redshifts $z \gtrsim 1$ at energies $E \gtrsim 10$ TeV, as the EBL opacity at those energies may be greatly reduced compared to standard-model predictions. Observations with the small-size telescopes of the future Cherenkov Telescope Array (CTA; Acharya et al. 2013)—and its predecessors, such as the Astrofisica con Specchi a Technologia Replicante Italiana (ASTRI; Vercellone 2016) array—will provide excellent opportunities to test this hypothesis.

We have presented, to the authors' knowledge for the first time, detailed calculations of the effect of LIV on the Compton scattering process. As for $\gamma\gamma$ absorption, we considered both subluminal and superluminal modifications to the photon dispersion relation. In the superluminal case, we find that for incoming photon energies of $E_{\gamma,i} \gtrsim 1$ PeV in the electron rest frame, both the electron recoil effect and the Klein–Nishina suppression of the scattering cross section are reduced compared to standard-model expectations. This may suggest that Compton scattering at ultra-high energies may overcome the suppression due to the standard Klein–Nishina effect and possibly lead to the production of $\gg 1$ PeV photons through inverse Compton scattering. However, it is unlikely that this effect is of relevance to realistic astrophysical environments. Such scattering would

require electrons of energies $E_e \gg 1$ PeV. In spite of the recovery at ultra-high energies, the Compton cross section is still suppressed by several orders of magnitude compared to the Thomson cross section. Hence, for any realistic magnetic field value in an astrophysical source, if electrons are actually accelerated to $E_e \gg 1$ PeV, or produced as secondaries in ultra-high-energy muon decay processes, they are likely to lose their energy radiatively via synchrotron radiation rather than Compton scattering. In the subluminal case, both the reduction of scattered photon energies and the Klein–Nishina cutoff of the cross section are further enhanced by the LIV effect, rendering Compton scattering at ultra-high energies even less efficient than due to the standard Klein–Nishina effects.

We thank the anonymous referee for a quick review and helpful suggestions. The work of M.B. is supported through the South African Research Chair Initiative of the National Research Foundation (NRF) and the Department of Science and Technology of South Africa, under SARChI Chair grant No. 64789. Any opinion, finding, and conclusion or recommendation expressed in this material is that of the authors and the NRF does not accept any liability in this regard.

ORCID iDs

Hassan Abdalla https://orcid.org/0000-0002-0455-3791
Markus Böttcher https://orcid.org/0000-0002-8434-5692

References

Abdalla, H., & Böttcher, M. 2017, ApJ, 835, 237
Abdallah, W., Delepine, D., Khalil, S., et al. 2013, PhLB, 725, 361
Acharya, B. S., Actis, M., Aghajani, T., et al. 2013, APh, 43, 3
Aharonian, F., Akhperjanian, A. G., Bazer-Bachi, A. R., et al. 2006, Natur, 440, 1018
Amelino-Camelia, G. 2013, LRR, 16, 05
Amelino-Camelia, G., Ellis, J., Mavromatos, N. E., Nanopoulos, D. V., & Sarkar, S. 1998, Natur, 393, 763
Arbab, A. I. 2015, Ap&SS, 355, 343
Azzam, W. J., Alothman, M. J., & Guessoum, N. 2009, AdSpR, 44, 1354
Biller, S. D., Breslin, A. C., Buckley, J., Catanese, M., & Carson, M. 1999, PhRvL, 83, 2108
Biteau, J., & Williams, D. A. 2015, ApJ, 812, 60
Capozziello, S., González, P. A., Saridakis, E. N., & Vásquez, Y. 2013, JHEP, 02, 039
Cole, S., Norberg, P., Baugh, C., et al. 2001, MNRAS, 326, 255
Dominguez, A., Primack, J. R., Rosario, D. J., et al. 2011a, MNRAS, 410, 2556
Dominguez, A., Sánchez-Conde, M. A., & Prada, F. 2011b, JCAP, 11, 020
Dzhatdoev, T. A. 2015, JPhCS, 632, 01
Dzhatdoev, T. A., Khalikov, E. V., Kircheva, A. P., & Lyukshin, A. A. 2017, A&A, 603, A59
El-Zant, A., Khalil, S., & Sil, A. 2015, PhRvD, 91, 035030
Essey, W., & Kusenko, A. 2010, APh, 33, 81
Fairbairn, M., Nilsson, A., Ellis, J., Hinton, J., & White, R. 2014, JCAP, 1406, 005
Finke, J. D., Razzaque, S., & Dermer, C. D. 2010, ApJ, 712, 238
Franceschini, A., Rodigheiro, G., & Vaccari, M. 2008, A&A, 487, 837
Furniss, A., Stutter, P. M., Primack, J. R., & Dominguez, A. 2015, MNRAS, 446, 2267
Furniss, A., Williams, D. A., Danforth, C., et al. 2013, ApJL, 768, L31
Gilmore, R. C., Sommerville, R. S., Primack, J. R., & Dominguez, A. 2012, MNRAS, 422, 3189
Hauser, M. G., & Dwek, E. 2001, ARA&A, 39, 249
Jacob, U., & Piran, T. 2008, PhRvD, 78, 124010
Jacobson, T., Liberati., S., & Mattingly, D. 2003, Natur, 424, 1019
Keenan, R. C., Barger, A. J., & Cowie, L. L. 2013, ApJ, 775, 62
Kudoda, A. M., & Faltenbacher, A. 2017, MNRAS, 467, 2896
Liberati, S., & Maccione, L. 2009, ARNPS, 59, 245
Lorentz, M., & Brun, P. 2017, EPJWC, 136, 03018
Matsuura, S., Arai, T., Bock, J. J., et al. 2017, ApJ, 839, 7
Mazin, D., Domínguez, A., & Fallah, R. V. 2017, in AIP Conf. Proc. 1792, High Energy Gamma-Ray Astronomy, 6th International Meeting on High Energy Gamma-Ray Astronomy, ed. F. A. Aharonian, W. Hofmann, & F. M. Rieger (Melville, NY: AIP), 050037
Nashed, G. L., & El Hanafy, W. 2014, EPJC, 74, 3099
Nikishov, A. I. 1962, JETP, 14, 393
Primack, J. R., Bullock, J. S., & Somerville, R. S. 2005, in AIP Conf. Proc. 745, High Energy Gamma-Ray Astronomy, ed. F. A. Aharonian, H. J. Völk, & D. Horns (Melville, NY: AIP), 23
Razzaque, S., Demer, C. D., & Finke, J. D. 2009, ApJ, 697, 483
Riess, A. G., Filippenko, A. V., Challis, P., et al. 1998, AJ, 116, 1009
Sami, H., Namane, N., Ntahompagaze, J., Elmardi, M., & Abebe, A. 2018, IJGMM, 15, 02
Schaefer, B. E. 1998, PhRvL, 82, 4964
Stecker, F. W. 1969, ApJ, 157, 507
Stecker, F. W., de Jager, O. C., & Salamon, M. H. 1992, ApJL, 390, L49
Sushkov, A. O., Kim, W. J., Dalvit, D. A. R., & Lamoreaux, S. K. 2011, PhRvL, 107, 171101
Sutter, P. M., Lavaux, G., Wandelt, B. D., & Weinberg, D. H. 2012, ApJ, 761, 44
Tavecchio, F., & Bonnoli, G. 2016, A&A, 585, A25
Vercellone, S. 2016, EPJWC, 121, 04006
Wanas, M. I., & Hassan, H. A. 2014, IJTP, 53, 3901
Wei, J., Zhang, B., Shao, L., et al. 2017, ApJL, 834, L13
Zemcov, M., Smidt, J., Arai, T., et al. 2014, Sci, 346, 732